The collective dynamics of NF − κB in cellular ensembles

Article *in* The European Physical Journal Special Topics · October 2018

DOI: 10.1140/epjst/e2018-800014-7

2 authors, including:

Ram Ramaswamy
Jawaharlal Nehru University
254 PUBLICATIONS **4,694** CITATIONS

Eur. Phys. J. Special Topics **227**, 851–863 (2018)

https://doi.org/10.1140/epjst/e2018-800014-7

THE EUROPEAN PHYSICAL JOURNAL SPECIAL TOPICS

Regular Article

The collective dynamics of NF−κB in cellular ensembles

Cluster synchrony, splay states, and chimeras

Raviteja Donepudi[1,a] and Ram Ramaswamy[1,2]

[1] Department of Biotechnology and Bioinformatics, School of Life Sciences, University of Hyderabad, Hyderabad 500046, India
[2] School of Computational and Integrative Sciences, Jawaharlal Nehru University, New Delhi 110067, India

Received 31 January 2018 / Received in final form 10 March 2018
Published online 19 October 2018

Abstract. The transcription factor NF−κB is a crucial component in inflammatory signalling. Its dynamics is known to be oscillatory and has been extensively studied. Using a recently developed model of NF−κB regulation, we examine the collective dynamics of a network of NF−κB oscillators that are coupled exogenously by a common drive (in this case a periodically varying cytokine signal corresponding to the TNF molecule concentration). There is multistability owing to the overlapping of Arnol'd tongues in each of the oscillators, and thus the collective dynamics exhibit a variety of complex dynamical states. We also study the case of a globally (mean field) coupled network and observe that the ensemble can display global synchronisation, cluster synchronisation and splay states. In addition, there can be dynamical chimeras, namely coexisting synchronised and desynchronized clusters. The basins of attraction of these different collective states are studied and the parametric dependence in the basin uncertainty is examined.

1 Introduction

Rhythmic phenomena in biological systems occur on a wide range of time-scales, from the millisecond level firing in neuronal systems to cycles of decades or more that are seen in ecology [1–6]. These rhythms are maintained by biological oscillators of various kinds [7], and their mutual interactions have been of considerable recent interest. Numerous phenomena at the cellular and subcellular levels are oscillatory, and many forms of control and signalling within biological cells are known to depend on periodicities in the expression levels of key molecular components [5–9].

Our interest in this work is on the collective dynamics of a group of oscillators that model the intracellular dynamics of an ubiquitous transcription factor, NF−κB [10,11]. Since stochasticity and nonlinearity are both very significant in a cellular

[a] e-mail: donepudiraviteja@gmail.com

environment, we examine a model of NF−κB dynamics that is known to have complex chaotic dynamics and investigate emergent behaviour in an ensemble of such systems.

The transcription factor NF−κB has a profound impact at the cellular and tissue levels, and has a significant effect at the physiological level as well [10]. Diverse signals appear to be mediated via NF−κB: cell survival, cell proliferation [12], development [13], the maintenance of the immune system [14], inflammation response [15], and so on. These phenomena clearly involve the concerted effects of both intracellular oscillators and intercellular communication.

These aspects motivate the present study of dynamics in an ensemble of coupled NF−κB networks. Most natural systems are not isolated, and thus one motivation for the present work is to examine the effect of coupling on the dynamics. Indeed the case of coupled networks (or even a network of networks) is likely to be the natural setting, when the interaction between systems leads to their having a high degree of dynamical correlation.

At the same time, studies on the dynamics of nonlinear systems have shown that there can be several forms of complex individual as well as collective dynamics. For instance, there may be more than one attractor of the dynamics so that different asymptotic states can coexist. Bi- (or multi-) stability can arise autonomously [16], or can result from the coupling [17,18]. When the multistability is induced, the coupled system can display a variety of novel dynamical behaviours, ranging from global synchrony to cluster synchrony and splay states [19,20], some of which have found parallels in biological dynamics [21,22]. Indeed, in such cases synchrony may well be essential for their proper functioning [23].

This paper is organized as follows. The model NF−κB network studied here is described in detail in Section 2. Developed over the past few years by Jensen, Krishna and co-workers [24,25], this model has been studied in great detail; see [26] for a recent summary. All essential molecules that are involved in the network have been incorporated in this somewhat minimalistic model (details of which are given below). We explore the dynamics of a single regulatory network and describe the occurrence of multistability, the basins of attraction of the different attractors and their geometry. The collective dynamics of an ensemble of such externally coupled networks is discussed in Section 3, followed by a study of globally mean-field coupled NF−κB networks. We conclude in Section 4 with a discussion and summary of our main results.

2 NF−κB model dynamics

Jensen and Krishna [25,26] introduced the following reduced model of the NF−κB network that captures the essential features of the dynamics. It consists of a set of five coupled differential equations,

$$\begin{aligned}
\dot{x} &= V_x(N_x - x)\frac{K_z}{K_z + z} - V_z z\frac{x}{K_x + x} \\
\dot{y} &= \Gamma_y x^2 - \Delta_y y \\
\dot{z} &= \Gamma_z y - \Delta_z u(N_x - x)\frac{z}{K_z + z} \\
\dot{u} &= \Gamma_u \tau w - \Delta_u u \\
\dot{v} &= \Delta_u u - V_v v\frac{K_A}{K_A + A_{20}\tau} \\
\tau &= A_0 + A\sin\left(\frac{2\pi}{T}t\right) \\
w &= N_{uv} - u - v,
\end{aligned} \tag{1}$$

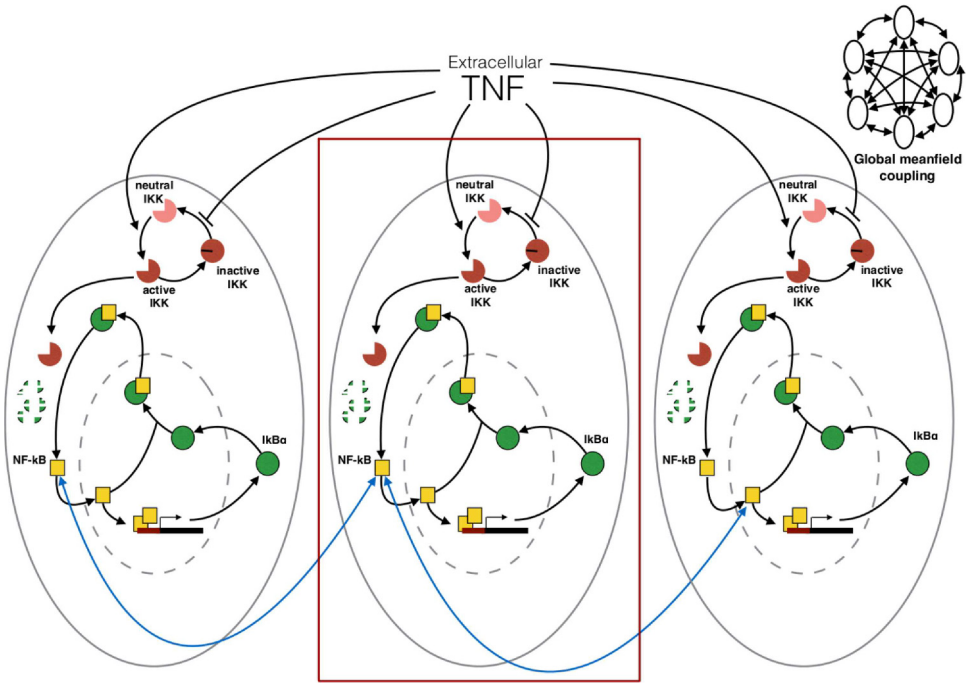

Fig. 1. Schematic of an individual NF−κB network (see the central panel) coupled to other similar networks. Within the cell nucleus NF−κB promotes the production of IκBα which then binds to NF−κB, generating negative feedback. External TNF (common to all cells) drives IKK oscillations as indicated. In its active form, IKK in the cytoplasm helps to degrade bound IκBα, freeing up the NF−κB which is then transported into the nucleus. These coupled feedback loops effectively cause NF−κB oscillations. We also consider a global mean-field coupling through NF−κB itself (denoted by the blue arrows) which connects all the networks. Each cell is coupled to all other cells, as indicated schematically in the top right corner inset.

wherein the variables represent concentrations of select components of the NF−κB module. In addition to the NF−κB protein, these include the inhibitor IκB, the tumor necrosis factor (TNF) and the enzyme IKK, which is a kinase; see Figure 1 for a schematic of the network.

We briefly discuss the role of the key molecular species that are involved in the network. TNF is a cytokine with both pathological and physiological functions [27–29]. While its primary role is to stimulate inflammatory response during infection, but it also plays role in apoptosis as well as necrosis [28,30]. TNF binds to the receptors TNFR1 and TNFR2 which are produced in many tissues. This binding leads to conformation changes that activate the NF−κB and MAPK pathways [28] and signalling of apoptosis. The cellular protein IκBα binds to NF−κB dimers to sterically prevent NF−κB from entering the nucleus [31]. In order that the NF−κB protein moves into the nucleus where it can carry out its function, the sequential phosphorylation, ubiquitination, and degradation of IκBα is essential [31,32]. Some of these latter actions such as the phosphorylation of IκB and NF−κB proteins are accomplished via signals from NF−κB activating stimuli such as the IκB kinase (IKK) that is composed of the two serine-threonine kinases (IKKα and IKKβ) and a regulatory subunit (IKKγ) [32]. Clearly all these molecules play a crucial role in the nuclear localisation and activation of NF−κB.

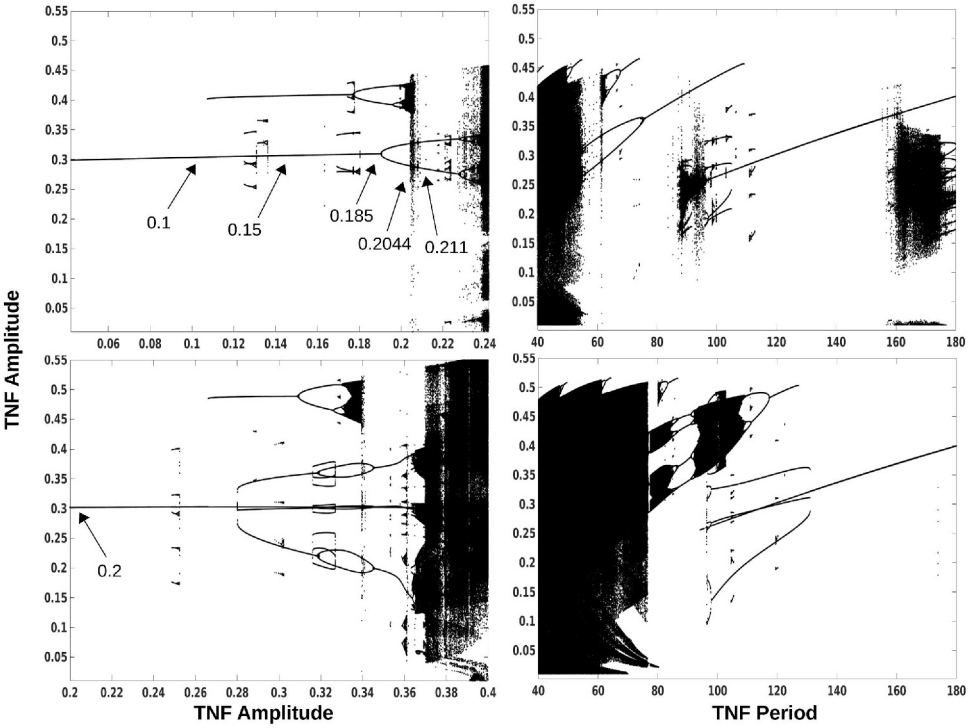

Fig. 2. Bifurcation diagram as a function of the TNF amplitude for periods a) $T = 60$ (top left), and c) $T = 120$ (bottom left), and as a function of the period T for fixed amplitudes b) $A = 0.211$ (top right) and d) $A = 0.3$ (bottom right). Plotted on the ordinate in all panels are the maxima of the NF$-\kappa$B concentration, namely x, over a sufficiently large number of oscillations.

The notation is as follows [25]: x, y, and z are respectively the concentrations of the nuclear NF$-\kappa$B protein, I-κB RNA and I-κB. The external TNF concentration τ is periodically modulated with time period T. This affects the dynamics of the neutral IKK w through its action on the active and inactive forms of IKK, denoted u and v respectively. As can be noted, the above equations describe a feedback loop in (x, y, z) coupled to the (u, v, w) system that is externally driven by the autonomous and periodic TNF oscillator.

The dynamics that results from the above five equations has been extensively studied by Jensen and co-workers in a series of papers [26,33–35]. It was recently shown [26] that depending on the modulation, there can be bistability in the system as a consequence of the overlapping of Arnold tongues: different initial conditions can correspond to different resonances.

We recall the main dynamical features of this system [25,35,36]. It is convenient to examine a bifurcation diagram that results from a variation of the parameters of the external modulation, namely A and T, the amplitude and period of TNF variation respectively. The bifurcation diagram is obtained in the standard way: the equations of motion are integrated, transients are discarded and a large number of successive maxima of the NF$-\kappa$B oscillations, namely the variable x are plotted subsequently. Several initial conditions are chosen for each value of the parameters so that bistability or multistability is immediately apparent. Figure 2, which is representative, has the following features. When the period is fixed and the amplitude is varied (panels on the left), there are extensive regions of multistability that occur subsequent to

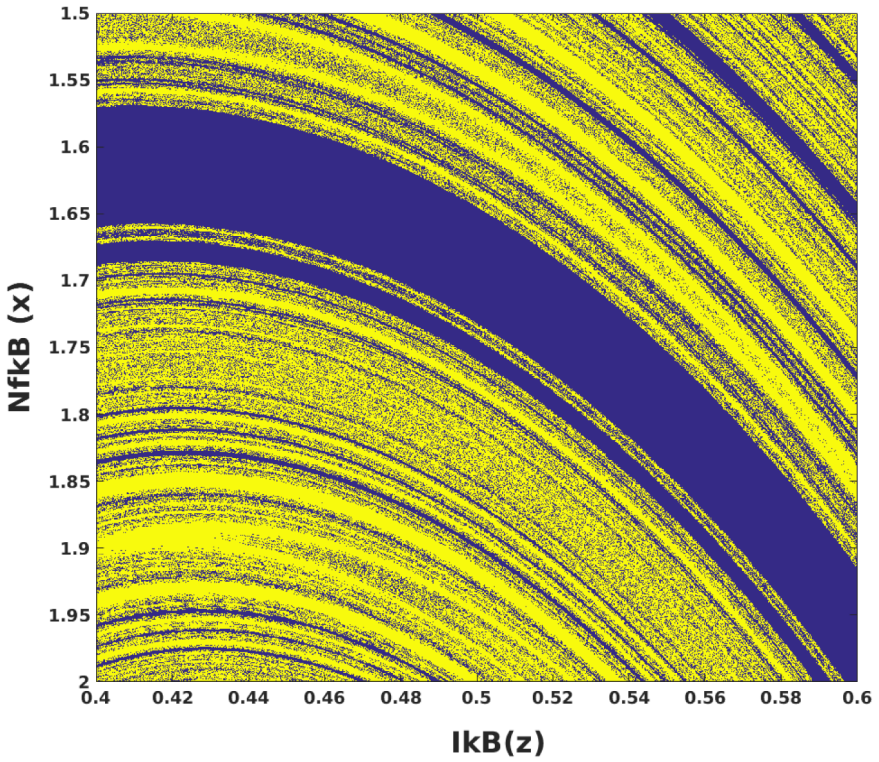

Fig. 3. Basins of attraction for the two coexisting attractors at $A = 0.2042$ and $T = 60$. The blue points are attracted to a chaotic attractor while the yellow points go to a limit cycle.

period-doubling bifurcations and these appear to be of two basic types: there can be coexistence of periodic orbits (namely limit cycles) of different periods as well as periodic orbits coexisting with more complex dynamics, namely chaotic orbits. Very similar behaviour is seen if the amplitude is fixed and the period is varied (the panels on the right; the choice of $A = 0.211$ and $A = 0.3$ is representative). In our simulations we follow earlier studies [26] and use the following values for the several parameters in the model: $V_x = 5.4$, $N_x = 1$, $K_z = 0.035$, $V_z = 0.018$, $K_x = 0.029$, $\Gamma_y = 1.03$, $\Delta_y = 0.017$, $\Gamma_z = 0.24$, $\Delta_z = 1.05$, $\Gamma_u = 0.24$, $N_{uv} = 2.0$, $\Delta_u = 0.18$, $V_v = 0.036$, $A_{20} = 0.0026$, $K_A = 0.0018$, and $A_0 = 0.5$.

We have examined the dynamics at several values of the period T and find that there typically is a region where two limit cycles coexist. In addition, there can be exterior crises, leading to a chaotic region. The basins of attraction in the region of multistability appears to be highly mixed (we discuss the characterization below). For $A = 0.2042$ and $T = 60$, there are two coexisting limit cycles owing to the overlapping Arnold tongues [26]. Points leading to the different attractors are shown in blue and yellow in Figure 3, for a small patch of initial conditions on the $x - z$ plane.

2.1 Attractor basins: boundary fractality and entropy

When the dynamics displays bistability or multistability, the nature of the attractor basins is naturally of interest. The manner in which the basins are arranged in the

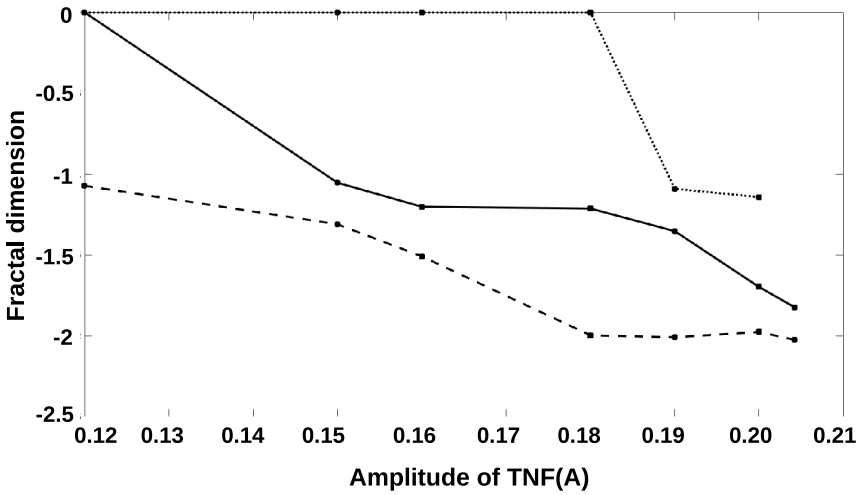

Fig. 4. Fractal dimension of the basins as computed from the basin entropy, as a function of the TNF period and amplitude. Calculations were done for selected amplitudes and periods $T = 45$ (dashed), 60 (solid) and 70 (dotted line).

phase space has a major effect on the dynamics of an ensemble of such oscillators, especially when they may be described as being intertwined or intermingled [37–39]. In such cases the prediction of the eventual attractor for a set of initial conditions can be difficult, and a recently proposed measure, the basin entropy, attempts to quantify this uncertainty [40].

Following the procedure specified by Daza et al. [40], the basin entropy is computed by first classifying a set of points inside a box of initial conditions by their corresponding final states. We thus determine the number of initial conditions going to each attractor, and this is then used to calculate the Boltzman entropy

$$S_i = -\sum_{j=1}^{m_i} p_{ij} \ln p_{ij},$$

where m_i is the number of attractors in the ith box and p_{ij} is the probability of the jth attractor in that box. The basin entropy at a particular scale ε is the average of S_i for all boxes, namely

$$S_b(\varepsilon) = \frac{1}{N} \sum_{i=1}^{N} S_i.$$

The uncertainty coefficient α, the exponent in the scaling behaviour of S_b,

$$S_b(\varepsilon) \sim \varepsilon^{\alpha},$$

can be numerically estimated as the slope in a log-log plot of S_b versus ε. Similarly the fractal dimension d_b is determined from the scaling of the fraction F_b of points in the boxes, $F_b(\varepsilon) \sim \varepsilon^{-d_b}$.

We find that in this system, the basin uncertainty increases as a function of the TNF amplitude: see Figures 4 and 5 (right panels). This indicates that the dynamics of an ensemble is likely to become more complex as the external TNF amplitude is increased whereas there is a decrease in entropy when the period of modulation is

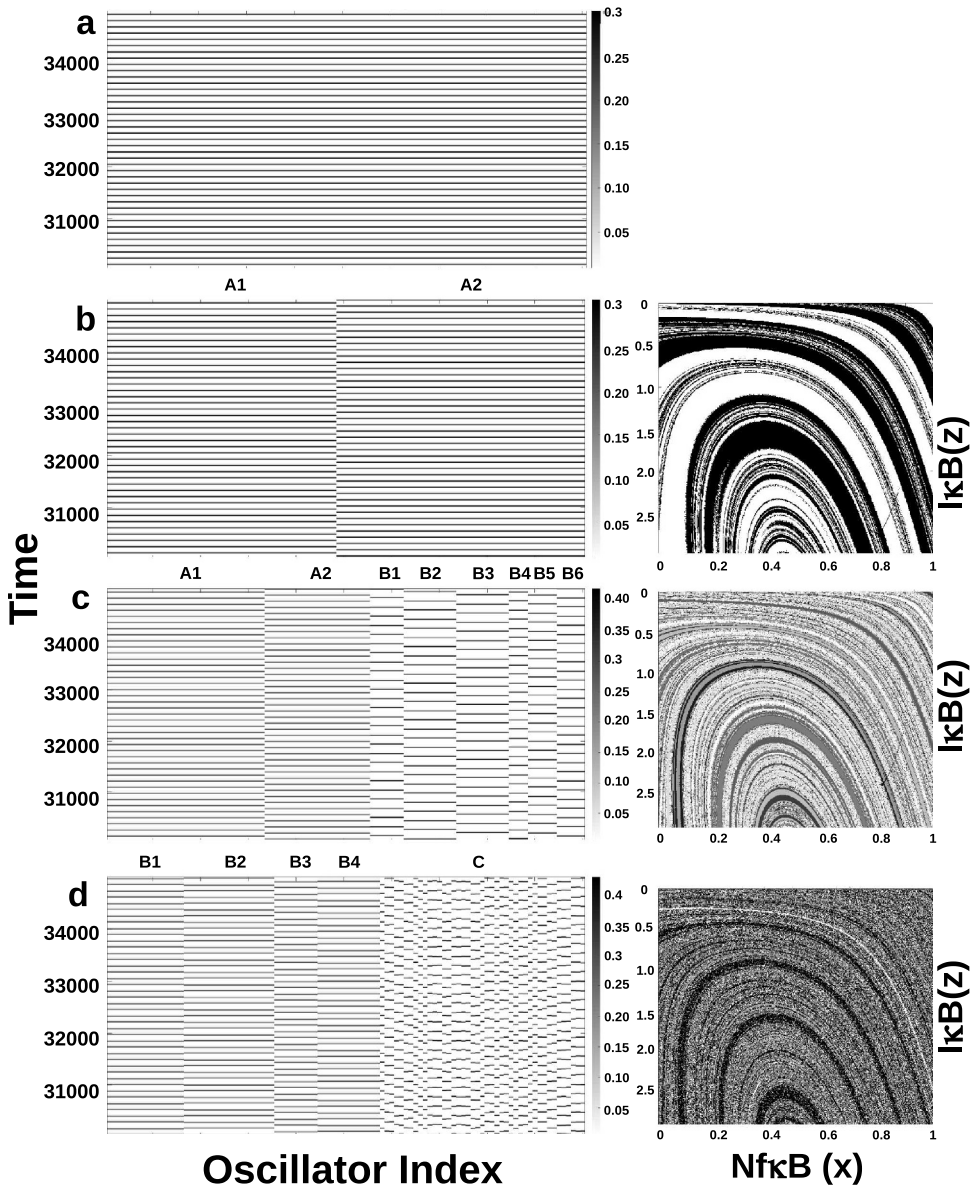

Fig. 5. Dynamics in the coupled networks of $N = 100$ NF$-\kappa$B oscillators. The values of the TNF amplitude and period are a) $T = 120$, $A = 0.2$, b) $T = 60$, $A = 0.15$, c) $T = 60$, $A = 0.185$, and d) $T = 60$, $A = 0.2042$ respectively. The basins of attraction for the different states are shown on the right, while on the left is a space-time plot in a time interval. The maxima of the different oscillators are shown, and one can clearly identify the different clusters that are formed. Note the coexistence of coherent clusters and an asynchronous set in d).

increased. This correlates with earlier experimental observations by Kellog and Tay [36] that reduced doses and large periods of TNF leads to synchronous oscillations and improved entrainment. As seen in our simulations, when A is low and T is large, namely the TNF oscillations have a small amplitude and large periods, the attractor basins are well separated and would therefore be more immune to noise-induced hopping, leading to better entrained and synchronous populations.

3 Dynamics of coupled NF−κB networks

We first examine the dynamics of an ensemble of NF−κB networks which are all indirectly coupled through a common TNF oscillator: see Figure 1. The equations of motion for this system are

$$\begin{aligned}\dot{x_i} &= V_x(N_x - x_i)\frac{K_z}{K_z + z_i} - V_z z_i \frac{x_i}{K_x + x_i} \\ \dot{y_i} &= \Gamma_y x_i^2 - \Delta_y y_i \\ \dot{z_i} &= \Gamma_z y_i - \Delta_z u(N_x - x_i)\frac{z}{K_z + z_i},\end{aligned} \tag{2}$$

with the subscript $i = 1, 2, \ldots, N$ labeling the individual oscillators. The dynamics of TNF is governed by the equations of motion for the variables u, v, w and τ and these are as in equation (1). When the parameters are such that there is a single stable attractor, all the oscillators in the ensemble synchronise into a single cluster (Fig. 5a). It can also happen that splay states are formed, namely the oscillators separate into multiple groups that are phase locked with respect to each other. Figure 5b shows two clusters denoted A_1, and A_2. The dynamics of each oscillator is on the same period one limit cycle attractor, but the two clusters are phase-locked with respect to each other. Similarly we can find splay states for period 2 limit cycle and so on (not shown).

In addition to complete synchronization and splay states, in regions of multistability where all the attractors are not chaotic, the oscillators can also show cluster synchronization, with different subsets being attracted to different attractors. Figure 5c shows such a state, with blocks named A_1 and A_2 corresponding to the splay states of the period one attractor while B_1, B_2, B_3, B_4, B_5 and B_6 correspond to the splay states of the period two oscillator. Similarly we can find such cluster synchronised populations for various combinations of periodic limit cycles.

In multistable regions where chaotic and periodic attractors coexist, the ensemble breaks up into clusters of in-phase or phase locked synchrony coexisting with a group that is desynchronised. In Figure 5d, the blocks marked B_1, B_2, B_3 and B_4 represent the synchronised groups on period 2 attractors. All oscillators in the group denoted C are desynchronised and the dynamics is chaotic. Such complexity is not exceptional in this system: chimeric states of this general type, namely mixtures of synchronised and desynchronous chaotic dynamics can be found for a range of parameters.

The emergence of chimeras in an ensemble of identical oscillators forced by a common drive was also observed in a previous study of an ensemble of Lorenz oscillators [19,20], where the driving itself created multistability. Here, on the other hand, multistability is a consequence of the overlapping of the Arnold tongues and this leads to chimeras in the ensemble.

3.1 Globally coupled NF−κB oscillators

We now consider the case when all oscillators interact through a global mean-field diffusive coupling in NF−κB. The dynamical equations are thus modified to

$$\dot{x_i} = V_x(N_x - x_i)\frac{K_z}{K_z + z_i} - V_z z_i \frac{x_i}{K_x + x_i} + \frac{K}{N-1}\sum_{j \neq i}(x_j - x_i), \tag{3}$$

where K is the strength of coupling between oscillators, N is total number of oscillators and the subscripts i and j label the individual oscillators.

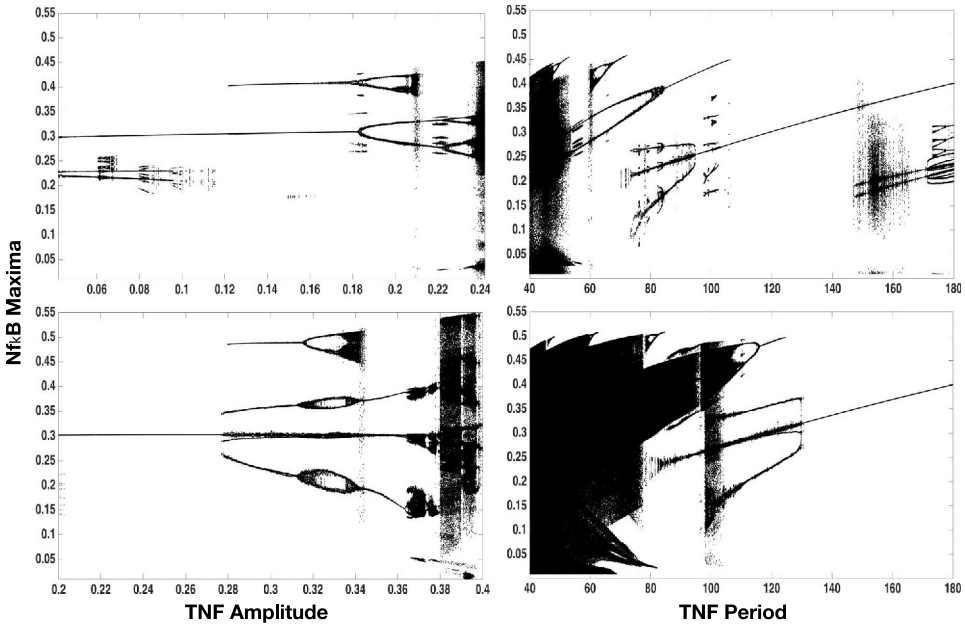

Fig. 6. Bifurcation diagram for mean-field coupled NF−κB oscillators with $K = 0.005$ as a function of the TNF amplitude for fixed periods, $T = 60$ (top-left) and $T = 120$ (bottom-left), and as a function of the TNF Period for fixed amplitude $A = 0.2011$ (top-right) and $A = 0.3$ (bottom-right). The ensemble contains $N = 64$ oscillators.

The ensemble dynamics can be significantly affected at even low coupling as can be seen in the bifurcation diagram, Figure 6. The variation with A is similar in overall structure to the uncoupled case, although new bifurcations can clearly be created. This differential influence of the coupling can lead to the establishment of newer multistable regions and also their loss. One such instance occurs at $A = 0.209$, where the coupling leads to the creation of a chaotic attractor in addition to the existing period two attractor. At this point of multistability, the ensemble shows a weak chimera [41], namely a partial frequency synchronisation in chaotic orbits. The oscillators on the period two limit cycle and chaotic attractor are organised into splay states. In Figure 7c the blocks denoted by B_1, B_2, B_3 and B_4 represent splay states of the period two attractor while the dynamics in the cluster marked C_0 is desynchronised chaotic motion. A scatter plot of NF−κB maxima between all possible pairs of oscillator groups shows the difference between phase synchronisation, splay states and weak chimeras.

To understand the effect of increasing coupling we coupled a population of 100 oscillators by mean-field coupling and observed the population behaviour at various coupling strengths. We chose $A = 0.209$ where there is a single period 2 attractor and population is spliced into 4 synchronised groups, with two peaks at around 0.33 and 0.29 (Figs. 7a and 8a). We started with a very low normalised coupling constant of $K = 0.001$, the population behaviour is same as before a 4 spliced synchronization and no new peaks are created (Figs. 7b and 8b). At $K = 0.005$ the population showed a chimera state (Fig. 7c). The populations is broken into two groups. One is represented by splay states of period two attractor, with peaks at around 0.33 and 0.29 (Fig. 8c). The other group is represented by chaotic orbits with mean peak at around 0.4 (Fig. 8d). At $K = 0.05$ coupling the population is organised into 4 groups (Fig. 7d). First two are synchronised to two different period two attractors (Fig. 8e). The third

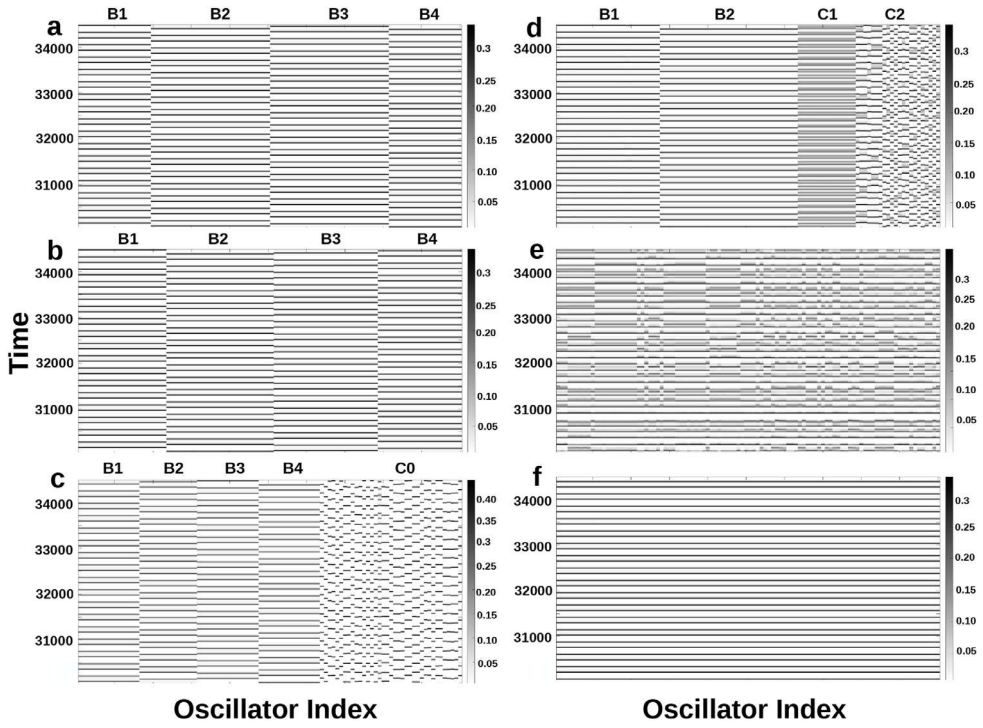

Fig. 7. Heat plot (as in Fig. 5, left panels) for an ensemble of 100 globally coupled oscillators for TNF period $T = 60$ and amplitude $A = 0.209$. The different panels correspond to coupling a) $K = 0$, b) $K = 0.001$ (cluster synchrony), c) $K = 0.005$ (chimera), d) $K = 0.05$ (chimera), e) $K = 0.5$ (asynchrony), and f) $K = 2$ (full synchrony) respectively.

and fourth groups are highly chaotic, with oscillators in third group being highly synchronised (Fig. 8f) and fourth are not synchronised (Fig. 8g). Further increase in coupling led to more synchronised population but with highly chaotic orbits (at $K = 0.1$ and 0.5) (Figs. 7e and 8h). For even larger coupling, the entire population synchronises to period-2 oscillations (Figs. 7f and 8i).

4 Discussion and summary

In the present work we have examined the collective dynamics that emerge through the interaction of networks of the important transcription factor, NF$-\kappa$B. The fact that the dynamics of NF$-\kappa$B in a single cell is oscillatory offers the possibility that it leads to differential gene expression [24,33,35,42]. When in addition, there is bistability (or multistability), there is the possibility of dynamical switching; an effect that can arise is noise-induced hopping that can help a cell switch between high and low production states for defined genes, namely multiplexing [35]. Noise can lead to an incoherent population, as has been experimentally observed [35,43].

In addition to states of global synchrony, the present network shows complex organization: an ensemble of cells can separate into clusters, each of which is individually synchronized. There can also be splay states as well as chimeras, namely the coexistence of coherent and incoherent populations of oscillators. In the present system, there are two types of coupling: all cells are driven externally by the periodic variation of a key enzyme, TNF, and there can be a global mean field formed by the

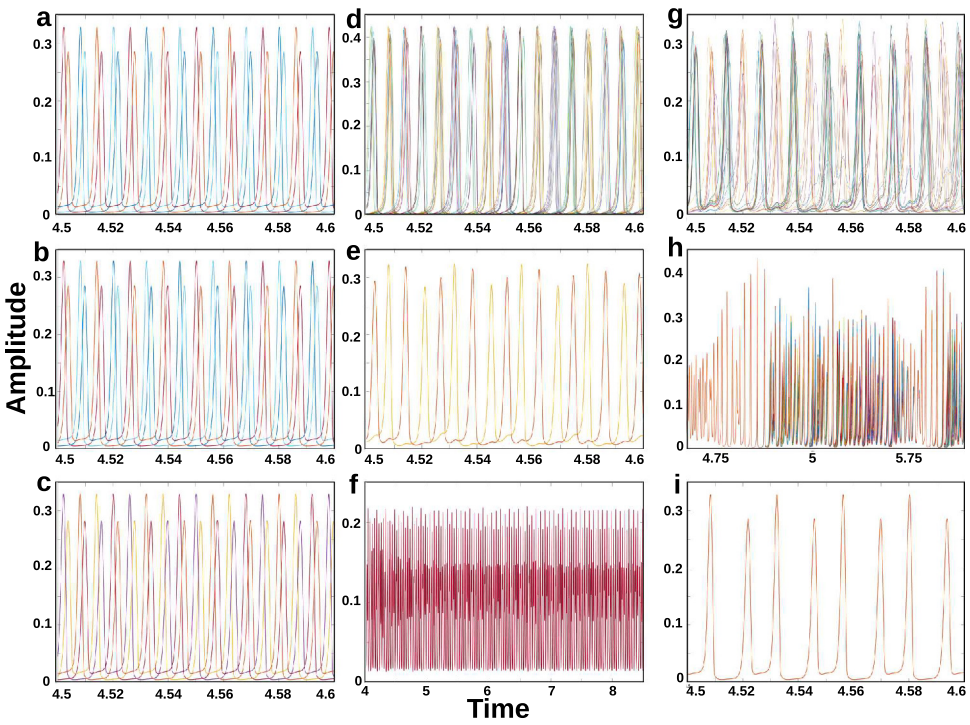

Fig. 8. Time series of the NF−κB oscillations in global mean-field coupled oscillators for fixed TNF period $T = 60$ and amplitude $A = 0.209$. The time is in units of 1000 seconds. a) Splay state for zero coupling, b) splay state for $K = 0.001$, c) period two splay for $K = 0.005$, d) asynchronous chaotic oscillations for $K = 0.005$, e) two groups of synchronised period-2 oscillators for $K = 0.05$, f) synchronised chaotic oscillators for $K = 0.05$, g) non-synchronised chaotic oscillations for $K = 0.05$, h) partially synchronised chaotic oscillations for $K = 0.5$, and i) fully synchronised period 2 oscillations for $K = 2$. Note that the x-axes in panels f) and h) are different from the others.

NF−κB in all cells. In all these cases, we find that the basins of different attractors have a complex geometry, and while it is difficult to establish that they are riddled, the fractality of the basin boundaries would indicate that the final state is highly sensitive to initial conditions. By measuring the uncertainty coefficient of the basins, we find that the amplitude and period of TNF variation play an important role in determining the global dynamics. An increase in the amplitude increase the basin uncertainty, suggesting that the system sensitivity to noise will be amplified with increasing amplitude [35,36].

We conclude with some observations regarding the possible role of dynamical chimeras in biological systems. As has been pointed out by Pisarchik and Feudel [17] and Pecora and co-workers [23] among others, multistability in the dynamics may be an essential requirement in biological systems since this forms the basis of many switches [44,45]. Dynamical symmetries – such as the creation of global sychrony – and the breaking of such symmetries are both of fundamental importance in biology, especially in qualitative cellular transitions and decision-making [46]. Symmetry breaking is essential during development, immune response, hormesis etc. Dynamical chimeras, with both coherent and incoherent populations provide such an opportunity for cellular oscillators to break an existing symmetry, and this could play a role during inflammation and tissue repair, when both temporal and spatial synchrony

are envisaged in a cellular population [47,48]. Here multistability can play a crucial role.

D. Raviteja thanks the CSIR, India for the Shyama Prasad Mukherjee Fellowship. Ram Ramaswamy acknowledges the support of the Department of Science and Technology, India through the JC Bose National Fellowship.

References

1. C.M. Gray, P. König, A.K. Engel, W. Singer, Nature **338**, 334 (1989)
2. A. Hastings, T. Powell, Ecology **72**, 896 (1991)
3. R. Lev Bar-Or, R. Maya, L.A. Segel, U. Alon, A.J. Levine, M. Oren, Proc. Natl. Acad. Sci. **97**, 11250 (2000)
4. L. Stone, D. He, J. Theor. Biol. **248**, 382 (2007)
5. F. Jülicher, J. Prost, Phys. Rev. Lett. **78**, 4510 (1997)
6. A. Hoffmann, A. Levchenko, M.L. Scott, Science **298**, 1241 (2002)
7. A.T. Winfree, *The Geometry of Biological Time* (Springer-Verlag, New York, 2001)
8. J.C. Dunlap, Cell **96**, 271 (1999)
9. A. Nandi, C. Vaz, A. Bhattacharya, R. Ramaswamy, BMC Syst. Biol. **3**, 1 (2009)
10. M.S. Hayden, S. Ghosh, Genes Dev. **26**, 203 (2012)
11. Q. Zhang, M.J. Lenardo, D. Baltimore, Cell **168**, 37 (2017)
12. A.A. Beg, D. Baltimore, Science **274**, 782 (1996)
13. L.A.J. O'Neill, C. Kaltschmidt, Trends Neurosci. **20**, 252 (1997)
14. P.A. Baeuerle, T. Henkel, Annu. Rev. Immunol. **12**, 141 (1994)
15. T. Lawrence, Cold Spring Harb. Perspect. Biol. **1**, 1 (2009)
16. U. Feudel, Int. J. Bifur. Chaos **18**, 1607 (2008)
17. A.N. Pisarchik, U. Feudel, Phys. Rep. **540**, 167 (2014)
18. S.R. Ujjwal, N. Punetha, R. Ramaswamy, M. Agrawal, A. Prasad, Chaos **26**, 063111 (2016)
19. S.R. Ujjwal, N. Punetha, A. Prasad, R. Ramaswamy, Phys. Rev. E **95**, 032203 (2017)
20. T. Wontchui, J.Y. Effa, H.P.E Fouda, S.R. Ujjwal, R. Ramaswamy, Phys. Rev. E **96**, 062203 (2017)
21. A. Pikovsky, M. Rosenblum, J. Kurths, *Synchronization: A Universal Concept in Nonlinear Sciences* (Cambridge University Press, Cambridge, 2003)
22. S.H. Strogatz, *Nonlinear dynamics and chaos: with applications to physics, biology, chemistry, and engineering* (Perseus books, New York, 1994)
23. L.M. Pecora, F. Sorrentino, A.M. Hagerstrom, T.E. Murphy, R. Roy, Nat. Commun. **5**, 4079 (2014)
24. S. Krishna, M.H. Jensen, K. Sneppen, Proc. Natl. Acad. Sci. **103**, 10840 (2006)
25. M.H. Jensen, S. Krishna, FEBS Lett. **586**, 1664 (2012)
26. M.L. Heltberg, S. Krishna, M.H. Jensen, J. Stat. Phys. **167**, 792 (2017)
27. G. Olmos, J. Lladó, Mediators Inflammation **2014**, 861231 (2014)
28. W.-M Chu, Cancer Lett. **328**, 222 (2012)
29. S.I. Grivennikov, A.V. Tumanov, D.J. Liepinsh, A.A. Kruglov, B.I. Marakusha, A.N. Shakhov, T. Murakami, L.N. Drutskaya, I. Förster, B.E. Clausen, L. Tessarollo, B. Ryffel, D.V. Kuprash, S.A. Nedospasov, Immunity **22**, 93 (2005)
30. E.E Varfolomeev, A. Ashkenazi, Cell **116**, 491 (2004)
31. M. Karin, Oncogene **18**, 686 (1999)
32. M. Hinz, C. Scheidereit, EMBO Rep. **15**, 46 (2014)
33. B. Mengel, A. Hunziker, L. Pedersen, A. Trusina, M.H. Jensen, S. Krishna, Curr. Opin. Genet. Dev. **20**, 656 (2010)
34. M.H. Jensen, L.P. Kadanoff, S. Krishna, J. Stat. Phys. **167**, 792 (2017)
35. M.L. Heltberg, R.A. Kellogg, S. Krishna, S. Tay, M.H. Jensen, Cell Syst. **3**, 532 (2016)
36. R.A. Kellogg, S. Tay, Cell **160**, 381 (2015)

37. H.E. Nusse, J.A. Yorke, Science **271**, 1376 (1996)
38. J.C. Alexander, J.A. Yorke, Z You, I. Kan, Int. J. Bifur. Chaos Appl. Sci. Eng. **02**, 795 (1992)
39. J. Huisman, F.J. Weissing, Am. Nat. **157**, 488 (2001)
40. A. Daza, A. Wagemakers, B. Georgeot, D. Guery-Odelin, M.A.F. Sanjuan, Sci. Rep. **6**, 31416 (2016)
41. P. Ashwin, O. Burylko, Chaos **25**, 013106 (2015)
42. T.Y. Tsai, Y.S. Choi, W. Ma, J.R. Pomerening, C. Tang, J.E. Ferrell Jr., Science **321**, 126 (2008)
43. S. Zambrano, I. DeToma, A. Piffer, M.E. Bianchi, A. Agresti, eLife **5**, e09100 (2016)
44. D. Angeli, J.E. Ferrell Jr., E.D. Sontag, Proc. Natl. Acad. Sci. USA **101**, 1822 (2004)
45. E. Ullner, A. Zaikin, E.I. Volkov, J. Garcia-Ojalvo, Phys. Rev. Lett. **99**, 148103 (2007)
46. R. Li, B. Bowerman, Cold Spring Harb. Perspect. Biol. **2**, a003475 (2010)
47. M.M. Markiewski, J.D. Lambris, Am. J. Path. **171**, 715 (2007)
48. S. Halstenberg, A. Panitch, S. Rizzi, H. Hall, J.A. Hubbell, Biomacromolecules **3**, 710 (2002)